Solar Phys
DOI 10.1007/s11207-008-9315-4

Acoustic-Power Maps of Solar Active Regions with Direction Filters and Phase-Velocity Filters

Dean-Yi Chou · Zhi-Chao Liang · Ming-Hsu Yang · Ming-Tsung Sun

Received: 20 October 2008 / Accepted: 23 December 2008

Abstract We study the properties of power maps of solar acoustic waves filtered with direction filters and phase-velocity filters. A direction filter is used to isolate acoustic waves propagating in a narrow range of directions. The acoustic-power map of the waves filtered with a direction filter shows extended reduced-power features behind magnetic regions with respect to the wave direction. A phase-velocity filter is further applied to isolate waves with similar wave paths. In the power maps of the waves filtered with both a direction filter and a phase-velocity filter, a reduced-power image of a sunspot appears behind the sunspot with respect to the wave direction. The distance between the sunspot and the secondary image is consistent with the one-skip travel distance of the wave packet associated with the phase-velocity filter. The waves filtered with direction and phase-velocity filters at the location of the secondary image could be used to probe the sunspot. In the quiet Sun, spatial fluctuations exist in any acoustic-power map. These fluctuations are mainly caused by interference among modes with the same frequency. The fluctuations are random with two properties: They change rapidly with time, and their magnitude decreases with the square root of the number of frames used in computing the acoustic-power map.

Keywords Oscillations, solar · Helioseismology, observations · Active regions, magnetic fields · Waves, acoustic

D.-Y. Chou (✉) · Z.-C. Liang · M.-H. Yang
Department of Physics, National Tsing Hua University, Hsinchu, 30013, Taiwan, ROC
e-mail: chou@phys.nthu.edu.tw

Z.-C. Liang
e-mail: d9622811@oz.nthu.edu.tw

M.-H. Yang
e-mail: d9522807@oz.nthu.edu.tw

M.-T. Sun
Department of Mechanical Engineering, Chang-Gung University, Kwei-San, 33333, Taiwan, ROC
e-mail: mtsun@mail.cgu.edu.tw

Published online: 27 January 2009

1. Introduction

The interaction between solar acoustic waves and magnetic fields could change the property of acoustic waves. Observations show that the power of oscillations in magnetic regions is reduced in comparison with quiet regions (Woods and Cram, 1981; Lites, White, and Packman, 1982; Tarbell *et al.*, 1988). This phenomenon is best shown by acoustic-power maps – spatial distributions of time-averaged squared velocity. Observed acoustic-power maps show that the acoustic wave amplitude in magnetic regions is lower than that in the quiet Sun (Braun *et al.*, 1992; Hindman and Brown, 1998; Ladenkov *et al.*, 2002).

Several mechanisms may contribute to the observed power reduction in magnetic regions in acoustic-power maps. Here we divide them into three categories: absorption, emissivity reduction, and local suppression. The following three mechanisms fall into the first category, absorption: *i*) The mechanical energy of acoustic waves may be converted into thermal energy (heat) by the interaction with magnetic fields (Hollweg, 1988). *ii*) The acoustic waves may be converted, for example, by scattering, into modes that are beyond the detection range (Cally and Bogdan, 1993; Braun, 1995; Crouch and Cally, 2005; Gordovskyy and Jain, 2008). *iii*) The cutoff frequency could be modified in the magnetic region such that the amount of wave energy leaking into the outer atmosphere may change. Since we cannot observationally distinguish among these three mechanisms, hereinafter we refer to them as absorption caused by magnetic field. The second category is the emissivity reduction: The emission of acoustic waves may be reduced in magnetic regions compared with that in the quiet regions owing to the reduction in convection in magnetic regions (Parchevsky and Kosovichev, 2007). The third category is local suppression: The observed lower energy density in magnetic regions may be caused by a local change in observed wave amplitude, rather than a change in energy. Several mechanisms may result in the local change in observed wave amplitude. First, the Wilson depression may cause a smaller observed wave amplitude (Hindman, Jain, and Zweibel, 1997). Second, the eigenfunctions are smaller in magnetic regions (Gordovskyy and Jain, 2008). Third, a greater wave speed in magnetic regions results in a reduction in local wave amplitude because of the conservation of energy flux, which is proportional to the product of wave speed and the square of wave amplitude. Fourth, the modification in the line profile in magnetic regions may lead to a change in Doppler measurements (Wachter, Schou, and Sankarasubramanian, 2006; Rajaguru *et al.*, 2007). Since these four mechanisms, causing a smaller observed wave amplitude, occur only locally inside magnetic regions and do not extend beyond magnetic regions, hereinafter we call them the local suppression. In acoustic-power-map measurements, we cannot distinguish among absorption, emissivity reduction, and local suppression. It should be noted that the power change in magnetic regions is sensitive to the frequency of the p modes (Lindsey and Brain, 1998).

In this study, we use direction filters to isolate the waves propagating in a narrow range of directions to study the interaction between magnetic regions and the waves. The acoustic-power maps of the waves filtered with the direction filters show extended reduced-power features beyond the magnetic regions. The local suppression does not contribute to the reduced-power features because they are outside the magnetic regions. There is some similarity between the direction filter used here and the one-dimensional analysis in Cameron, Gizon, and Duvall (2008). We also apply a phase-velocity filter together with a direction filter to study the interaction between magnetic regions and the wave packets propagating in a particular direction.

In Section 2, we describe the data and preliminary reduction. In Section 3, we discuss the direction filters and the corresponding acoustic-power maps. In Section 4, we discuss

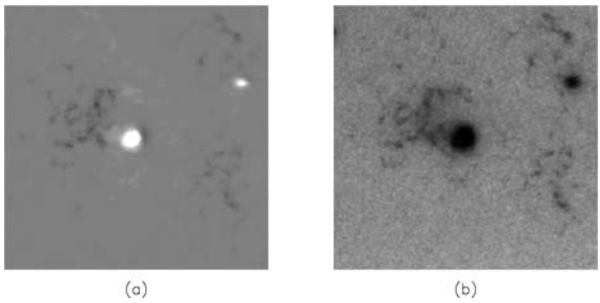

Figure 1 (a) Magnetic and (b) acoustic-power maps of active region NOAA 9057. No filter is applied here.

the acoustic-power maps of waves filtered with both direction and phase-velocity filters. In Section 5, we discuss the properties of spatial fluctuations of acoustic-power maps in the quiet Sun.

2. Data and Preliminary Reduction

In this study, we use the helioseismic data taken with MDI onboard the *Solar and Heliospheric Observatory* (Scherrer *et al.*, 1995). The data are 1024 × 1024 full-disk Dopplergrams taken at a rate of one image per minute. A time series of 4096 minutes taken in the period of 29 June to 2 July 2000 is used in this study.

The procedure of the preliminary data reduction is described as follows:

i) To remove the solar rotational velocity and slow temporal variations, the 61-frame running mean is subtracted from the measured signal at each spatial point.
ii) A temporal filter is applied to remove signals below 1.5 mHz.
iii) Each full-disk image is transformed into coordinates of longitude and latitude.
iv) The differential rotation of the solar surface is corrected (Chou *et al.*, 1999).
v) An area centered on the leading sunspot of NOAA 9057 is selected, and each image is transformed into a coordinate system of (ϕ, θ), centered on the sunspot center, where ϕ is East – West direction and θ the North – South direction. The dimension of the selected region is 30° in ϕ and 30° in θ, corresponding to 256 × 256 pixels. Each grid covers 0.117° × 0.117°.

In our computer codes, steps *iii*) – *iv*) are combined such that the spatial interpolation is carried out only once to minimize data degrading. The data cube after this procedure is ready for the following analysis. The acoustic-power map, computed by averaging the square of the oscillatory amplitude over time, is shown in Figure 1b. Hereinafter, the acoustic-power map without applying any filter is called the raw acoustic-power map. For comparison, we also show the line-of-sight magnetic map for the same period in Figure 1a. The sunspot at the center of the frame is the leading sunspot of NOAA 9057.

3. Acoustic-Power Maps with Direction Filters

A direction filter is used to isolate waves propagating in a small range of directions. In this study, we approximate an area of the solar surface by a plane. The coordinates (ϕ, θ) are approximated by the Cartesian coordinates (x, y). Each image is transformed to the Fourier domain (k_x, k_y). The direction filter in the Fourier domain is applied to isolate the waves

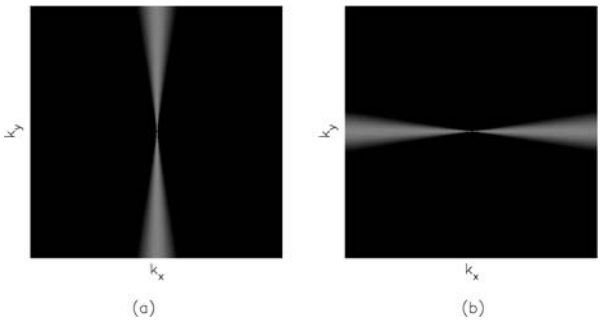

Figure 2 Two direction filters in the Fourier domain (k_x, k_y). The width is $\pm 15°$.

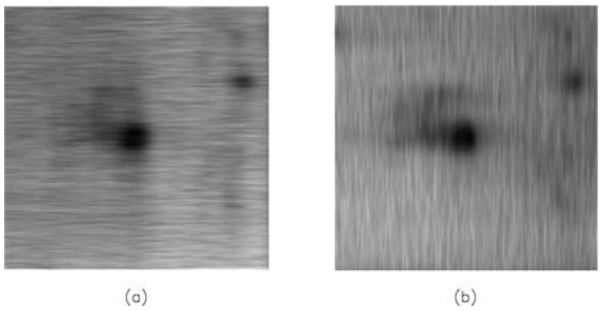

Figure 3 Power maps of the waves filtered with the direction filters in Figure 2: (a) waves propagating in the y-direction; (b) waves propagating in the x-direction.

propagating within a narrow range of a particular direction. Two examples of the filter in the Fourier domain (k_x, k_y) are shown in Figure 2. The filter shown in Figure 2a is nonzero only within $\pm 15°$ of the k_y-axis. A Hanning window in the k_x-direction is applied to reduce leakage. This filter isolates the waves propagating in the directions within $\pm 15°$ from the y-axis. Because of the Hanning window, 80% of the energy is confined within the central 37% of the width. Figure 2b is a filter isolating the waves propagating in the direction within $\pm 15°$ of the x-axis.

After the direction filter in the Fourier domain (k_x, k_y) is applied, each image is transformed back to the spatial domain (x, y). The acoustic-power map is computed by averaging the squared velocity over the time series. The acoustic-power maps corresponding to two filters in Figure 2 are shown in Figure 3.

We further isolate the waves propagating in the positive y-direction or the negative y-direction. The waves propagating in the positive y-direction consist of the components of $e^{i(\pm k_x x + k_y y - \omega t)}$ and $e^{i(\pm k_x x - k_y y + \omega t)}$, where k_x, k_y, and ω are positive. The corresponding acoustic-power map is shown in Figure 4a. The waves propagating in the negative y-direction consist of the components of $e^{i(\pm k_x x + k_y y + \omega t)}$ and $e^{i(\pm k_x x - k_y y - \omega t)}$. The corresponding acoustic-power map is shown in Figure 4b. The acoustic-power maps corresponding to the waves propagating in the positive and negative x-directions are shown in Figures 4c and 4d, respectively.

Acoustic-power maps in Figure 4 clearly show that the power deficit relative to the quiet Sun exists not only in the magnetic regions but also in an area beyond the magnetic regions. The power is lower in the area behind the magnetic regions with respect to the wave direction, while it is unchanged in the area in front of the magnetic regions. This indicates that the influence of the magnetic regions on wave energy extends beyond the magnetic regions as the waves pass through the magnetic regions. From the discussion in Section 1, absorption, emissivity reduction, and local suppression could contribute to the power deficit in the mag-

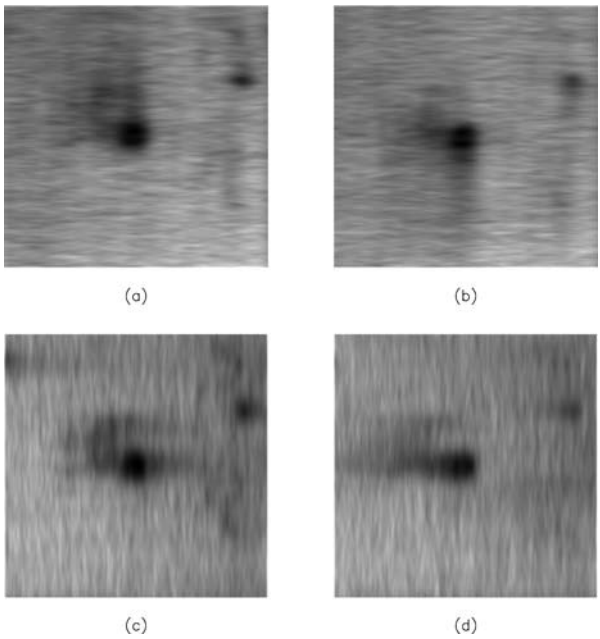

Figure 4 Power maps of the waves propagating in four different directions: (a) waves propagating in the positive y-direction, (b) waves propagating in the negative y-direction, (c) waves propagating in the positive x-direction, and (d) waves propagating in the negative x-direction. The width of the direction filters is $\pm 15°$.

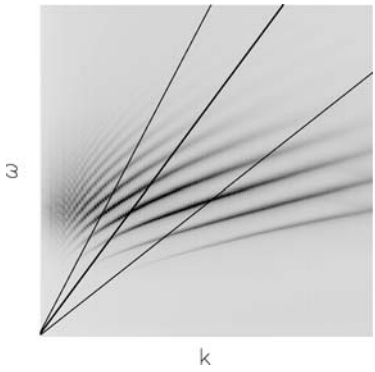

Figure 5 Phase-velocity filter in the $k-\omega$ diagram. The central straight line corresponds to the central angular phase velocity of the filter, $w_0 = 6.98 \times 10^{-5}$ rad s^{-1} (corresponding to $\ell = 300$ at 3.33 mHz). The other two lines indicate the width of the filter, $\delta w = 5.82 \times 10^{-5}$ rad s^{-1}.

netic regions, but only absorption and emissivity reduction could contribute to the power deficit in the extended regions. The extended reduced-power features behind the magnetic regions could be used to probe the interaction between the waves and the magnetic regions.

The extended features in the power maps in Figure 3 are weaker than those in Figure 4. This is because the waves in Figure 3a are the superposition of the waves in Figures 4a and 4b. After the waves propagating in the positive and negative y-directions are summed, the extended features in Figure 3a are diluted. This is also why the extended features are not seen in the raw acoustic-power maps in Figure 1b, because the waves in the raw power maps are the superposition of the waves propagating in all different directions.

The power maps in Figure 4 have striped features perpendicular to the propagation direction everywhere. These are caused by the narrow direction filter. The narrower the filter, the longer the striped feature. The spatial fluctuations of these power maps in the quiet Sun are random. Their properties are discussed in Section 5.

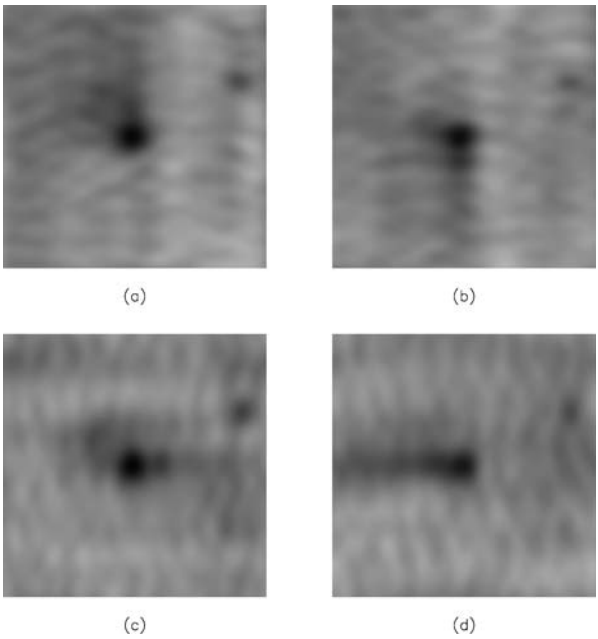

Figure 6 Power maps of the waves filtered with direction filters used in Figure 4 and a phase-velocity filter of $w_0 = 6.98 \times 10^{-5}$ rad s^{-1} (corresponding to $\ell = 300$ at 3.33 mHz) and $\delta w = 5.82 \times 10^{-5}$ rad s^{-1}, shown in Figure 5.

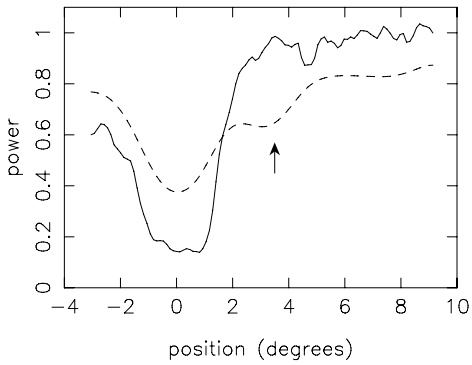

Figure 7 Power along a line in the x-direction through the center of the sunspot. The dashed line is for the power map in Figure 6c, and the solid line is for the power map in Figure 1b. The power is averaged over seven pixels in the y-direction. The location of the secondary image of the sunspot is indicated by an arrow. The power is normalized by the mean value in the quiet Sun.

4. Acoustic-Power Maps with Direction and Phase-Velocity Filters

In this section, besides the direction filter, we further apply a phase-velocity filter. A resonant p mode is trapped and multiply reflected in a cavity between the surface and a layer in the solar interior. The acoustic signal emanating from a point at the surface propagates downward to the bottom of the cavity and back to the surface at a different horizontal distance from the original point. Different p modes have different paths and arrive at the surface with different travel times and different distances from the original point. The modes with the same angular phase velocity w ($\equiv 2\pi\nu/\ell$, where ν is the mode frequency and ℓ the spherical harmonic degree) have approximately the same ray path and form a wave packet. In this study, we apply a Hanning phase-velocity filter to isolate the waves with phase velocity within the range of $(w_0 - \delta w/2, w_0 + \delta w/2)$, where δw is the width of the Hanning window. The corresponding FWHM is $\delta w/2$.

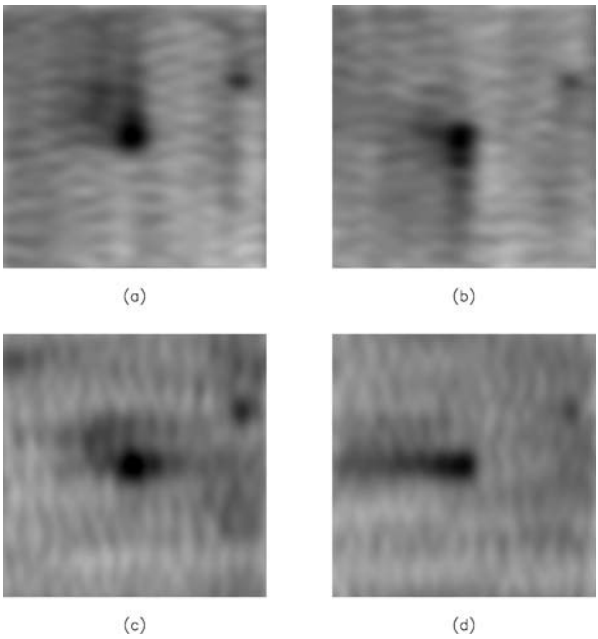

Figure 8 Power maps of the waves filtered with direction filters used in Figure 4 and a phase-velocity filter of $w_0 = 5.98 \times 10^{-5}$ rad s^{-1} (corresponding to $\ell = 350$ at 3.33 mHz) and $\delta w = 5.82 \times 10^{-5}$ rad s^{-1}. They look similar to those in Figure 6, but with a smaller separation between the secondary image and the sunspot.

An example of a phase-velocity filter is shown in Figure 5; here $w_0 = 6.98 \times 10^{-5}$ rad s^{-1} (corresponding to $\ell = 300$ at 3.33 mHz) and $\delta w = 5.82 \times 10^{-5}$ rad s^{-1}. The acoustic-power maps with this phase-velocity filter and the direction filters used in Figure 4 are shown in Figure 6. An interesting phenomenon in these power maps is that there is a black patch behind the leading sunspot of NOAA 9057. The black patch is clearly seen in Figures 6a, 6b, and 6c. In Figure 6d, the black patch is difficult to identify because it is mixed with the magnetic regions behind the sunspot.

The distance between the center of this black patch and the sunspot center is about 3.5°, which is consistent with the one-skip travel distance of the wave packet associated with w_0. Unlike the spatial fluctuations in the quiet Sun, which are random, this black patch behind the sunspot is stable and its magnitude does not decrease with the number of frames used in computing the power map. We believe that this black patch is the reduced-power image of the sunspot. The waves filtered with both direction filter and phase-velocity filter consist of many wave packets propagating in the same direction but with different phases. The wave packets with different phases are reflected at different locations on the surface. The wave packet that is reflected at the location of the sunspot has a lower energy because of absorption and emissivity reduction in the sunspot. When this wave packet returns to the surface after traveling one skip distance, its energy is still lower than the quiet Sun. Thus at the one-skip distance from the sunspot, its acoustic power is lower than the quiet Sun. We call this black patch the secondary image of the sunspot. To see the power in the secondary image of the sunspot, we plot the power in Figure 6c along a line in the x-direction through the center of the sunspot. The result is shown by the dashed line in Figure 7. The power is the average over seven pixels in the y-direction. The arrow indicates the location of the secondary image. For the comparison, we also plot the corresponding distribution for the raw power map in Figure 1b by the solid line in Figure 7.

Figure 8 shows the acoustic maps of the waves filtered with another phase velocity, $w_0 = 5.98 \times 10^{-5}$ rad s^{-1} (corresponding to $\ell = 350$ at 3.33 mHz) and $\delta w = 5.82 \times 10^{-5}$ rad s^{-1}.

There is also a secondary image behind the leading sunspot. The distance between the centers of the sunspot and the secondary is about 2.5°, which is consistent with the one-skip travel distance corresponding to $w_0 = 5.98 \times 10^{-5}$ rad s^{-1}. It is worth mentioning that phase-velocity filters could introduce artifacts in active regions, especially for small w_0 (Rajaguru *et al.*, 2006).

There are also spatial fluctuations in the quiet Sun for the power maps in Figures 6 and 8. The spatial scale of these spatial fluctuations is consistent with the one-skip travel distance corresponding to w_0. These fluctuations in the quiet Sun are random and are discussed in Section 5.

5. Spatial Fluctuations of Acoustic-Power Maps in the Quiet Sun

The acoustic-power maps show that the acoustic power in the quiet Sun is not completely uniform. For the power maps filtered with direction filters in Figures 3 and 4, there are striped features in the quiet Sun. For the power maps filtered with direction and phase-velocity filters in Figures 6 and 8, there are spatial fluctuations with a spatial scale consistent with the one-skip travel distance corresponding to w_0, the central phase velocity of the phase-velocity filter. Even for the raw power map in Figure 1, there are fluctuations in the quiet Sun. In this section, we discuss a possible source of the spatial fluctuations of power maps in the quiet Sun, besides observational noise.

The velocity field of acoustic waves, $\Psi(\mathbf{r}, t)$, can be expressed as the sum of Fourier components:

$$\Psi(\mathbf{r}, t) = \sum_{\mathbf{k},\omega} A(\mathbf{k}, \omega) \mathrm{e}^{\mathrm{i}\mathbf{k}\cdot\mathbf{r}} \mathrm{e}^{-\mathrm{i}\omega t}, \tag{1}$$

where $\mathbf{r} = (x, y)$ and $\mathbf{k} = (k_x, k_y)$. The intensity of the acoustic-power map is the time-averaged square of the velocity field over N frames:

$$\begin{aligned} P(\mathbf{r}) &= \frac{1}{N} \sum_t \left|\Psi(\mathbf{r}, t)\right|^2 = \frac{1}{N} \sum_t \sum_{\substack{\mathbf{k}\omega \\ \mathbf{k}'\omega'}} A(\mathbf{k}, \omega) A^*(\mathbf{k}', \omega') \mathrm{e}^{\mathrm{i}(\mathbf{k}-\mathbf{k}')\cdot\mathbf{r}} \mathrm{e}^{-\mathrm{i}(\omega-\omega')t} \\ &= \frac{1}{N} \sum_t \sum_{\mathbf{k}\omega} \left|A(\mathbf{k}, \omega)\right|^2 + \frac{1}{N} \sum_t \sum_{\mathbf{k}\neq\mathbf{k}'} \sum_{\omega} A(\mathbf{k}, \omega) A^*(\mathbf{k}', \omega) \mathrm{e}^{\mathrm{i}(\mathbf{k}-\mathbf{k}')\cdot\mathbf{r}} \\ &\quad + \frac{1}{N} \sum_t \sum_{\mathbf{k}\mathbf{k}'} \sum_{\omega\neq\omega'} A(\mathbf{k}, \omega) A^*(\mathbf{k}', \omega') \mathrm{e}^{\mathrm{i}(\mathbf{k}-\mathbf{k}')\cdot\mathbf{r}} \mathrm{e}^{-\mathrm{i}(\omega-\omega')t}. \end{aligned} \tag{2}$$

The second and third terms are the interference among the Fourier components. The third term vanishes because $\sum_t \mathrm{e}^{-\mathrm{i}(\omega-\omega')t} = 0$. Thus the intensity of the power map becomes

$$P(\mathbf{r}) = \sum_{\mathbf{k}\omega} \left|A(\mathbf{k}, \omega)\right|^2 + \sum_{\omega} \sum_{\mathbf{k}\neq\mathbf{k}'} A(\mathbf{k}, \omega) A^*(\mathbf{k}', \omega) \mathrm{e}^{\mathrm{i}(\mathbf{k}-\mathbf{k}')\cdot\mathbf{r}}. \tag{3}$$

The first term in Equation (3) is a constant without spatial dependence. The second term is the interference among the different Fourier components with the same frequency, hereinafter called the interference term. It depends on the spatial location and is nonzero even in the quiet Sun. It contributes to the observed spatial fluctuations of power maps in the quiet Sun.

The function $\Psi(x, y, t)$ in Equation (1) is the measured velocity, which includes not only the contribution from the p-mode and f-mode waves but also all other velocity sources, such as stochastic sources, turbulent convective velocity, and background velocity (Christensen-Dalagaard, 2005; Skartlien, 2002). Thus, the interference term in Equation (3) includes the contributions from p and f modes and all other velocity sources. It is noted that the Fourier components in the interference term include the modes on the p-mode and f-mode ridges as well as the nonresonant waves between ridges. The interference term consists of interference between any pair of Fourier components with the same ω. However, the major contribution comes from the interference between the components on the ridges because most of the power of the measured velocity is located on the ridges. This property can be demonstrated with the observed data as follows.

Here we select a quiet region with dimension of $30^\circ \times 30^\circ$ from the same data set. To demonstrate the effect of interference, we compute the power map of the waves filtered with a direction filter propagating in one direction and a phase-velocity filter because interference is relatively simpler in this limited range of the Fourier domain. Since p-mode power peaks at about 3.33 mHz, most contributions come from the signals around this frequency. We plot the power spectrum *versus* mode degree (ℓ) at 3.33 mHz for the waves filtered with a phase-velocity filter of $w_0 = 7.48 \times 10^{-5}$ rad s^{-1} (corresponding to $\ell = 280$ at 3.33 mHz) and $\delta w = 5.82 \times 10^{-5}$ rad s^{-1} in Figure 9a. Since most of power is located on the p_3 and p_4 ridges, the interference term comes mainly from the interference between p_3 and p_4 modes. Thus, the power map has a spatial scale corresponding to $\delta\ell$, where $\delta\ell$ is the difference between two ridges. For the phase-velocity filter in Figure 9a, $\delta\ell = 84$.

The spatial scale of the fluctuations of the power map could be understood from another point of view. From Equation (3), the spatial Fourier transform of the power map $P(\mathbf{k})$ can be expressed as

$$P(\mathbf{k}) = \frac{1}{N_x N_y} \sum_{\mathbf{r}} P(\mathbf{r}) \mathrm{e}^{-\mathrm{i}\mathbf{k}\cdot\mathbf{r}} = \sum_{\omega} \sum_{\mathbf{k}'} A(\mathbf{k} + \mathbf{k}', \omega) A^*(\mathbf{k}', \omega), \tag{4}$$

where N_x and N_y are the dimensions of x and y, respectively. Equation (4) simply states a familiar relation between the autocorrelation function and the Fourier transform of power spectra: The autocorrelation of $A(\mathbf{k}, \omega)$ at a fixed ω equals the spatial Fourier transform of the power map. Thus, for the power map of the waves filtered with a direction filter and a phase-velocity filter, the dominant spatial scale corresponds to $\delta\ell$, where $\delta\ell$ is the difference in ℓ between two dominant ridges as shown in Figure 9a. To check this property, we compute the spatial power spectrum of the power map filtered with a direction filter of $\pm 15^\circ$ propagating in the positive y-direction and a phase-velocity filter in Figure 9a, shown in Figure 9b. Besides the peak near $\ell = 0$, which corresponds to the large-scale nonuniformity, the power spectrum peaks at $\ell = 84$, which is equal to the difference between two dominant ridges in Figure 9a, $\delta\ell = 84$.

We test this property with another two phase-velocity filters. The results are shown in Figures 9c – 9f. They all agree with the relation that the power spectrum of the power map peaks at $\delta\ell$. The power peaks at $\ell = 180$ in Figures 9d and $\delta\ell = 168$ in Figure 9c. (Note that the resolution in ℓ is 12.) The power peaks at $\ell = 240$ in Figures 9f and $\delta\ell = 240$ in Figure 9e. Therefore, the major contribution of the spatial fluctuations of the power maps is from the interference between p modes with the same frequency. It is noted that the spatial scale of the fluctuations in the power map equals the one-skip travel distance of the wave packet associated with the phase-velocity filter. This can be understood with the relation between the $k - \omega$ diagram and the time – distance diagram (Bogdan, 1997).

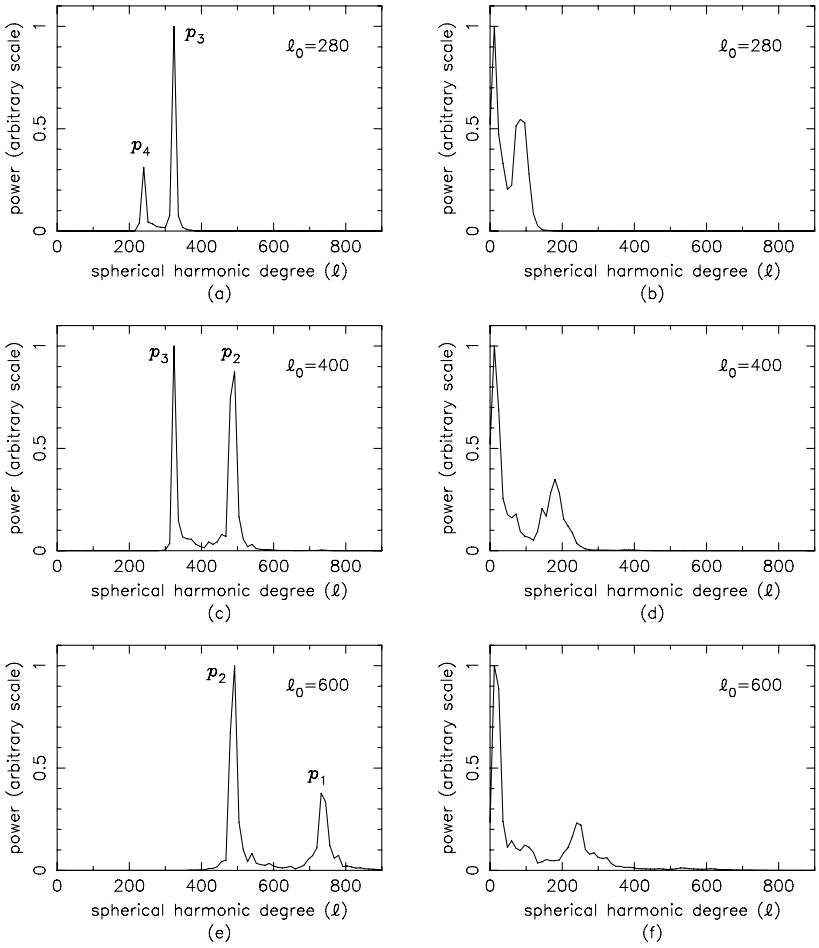

Figure 9 (Left) Power spectra *versus* ℓ at 3.33 mHz for the waves filtered with three different phase-velocity filters. (Right) Spatial power spectra of power maps for the waves filtered with a direction filter of $\pm 15^{\circ}$ and three different phase-velocity filters. (a) and (b) use a phase-velocity filter of $w_0 = 7.48 \times 10^{-5}$ rad s^{-1}, corresponding to $\ell = 280$ and 3.33 mHz (defined as ℓ_0 in the plot). (c) and (d) use a phase-velocity filter of $w_0 = 5.24 \times 10^{-5}$ rad s^{-1}, corresponding to $\ell = 400$ and 3.33 mHz. (e) and (f) use a phase-velocity filter of $w_0 = 3.49 \times 10^{-5}$ rad s^{-1}, corresponding to $\ell = 600$ and 3.33 mHz. The distance between two dominant ridges ($\delta\ell$) in the left panel is approximately equal to the location of peak power in the right panel.

Some of general properties of the interference term in Equation (3) can be derived as follows. Since the phases of $A(k_x, k_y, \omega)$ and $A^*(k'_x, k'_y, \omega)$ are random, the phase of the interference term is also random. That is, the spatial fluctuation pattern of power maps in the quiet Sun is random. The random spatial fluctuations have the following two properties. First, the fluctuation patterns change rapidly with time such that the correlation between two consecutive power maps is small. Second, the magnitude of the spatial fluctuations in the quiet Sun decreases as $N^{-1/2}$, where N is the number of frames used in computing the power map. If N frames are used in computing the power map, the number of points in the ω domain is equal to N. That is, the number of terms in the summation over ω in the

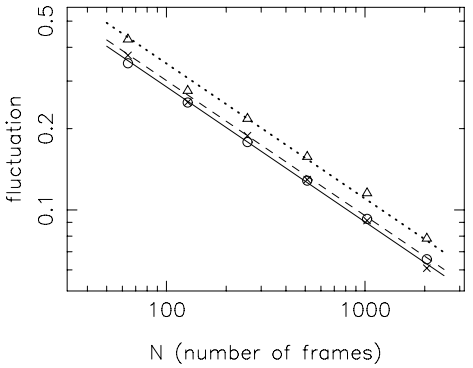

Figure 10 Magnitude of spatial fluctuations *versus* number of frames (N), for three acoustic-power maps: raw power map (circle and solid line), power map with direction filter (cross and dashed line), and power map with both direction and phase-velocity filters (triangle and dotted line). The straight line corresponds to $N^{-1/2}$ passing through the third point for each case.

interference term is equal to N. Since the phase before summing over ω is random, the magnitude of the interference term should decrease as $N^{-1/2}$.

The two properties of randomness hold for any acoustic-power map no matter what filter is applied. Here, we use a $15^\circ \times 15^\circ$ region in the quiet Sun to test these two properties. To test the first property, we compute the correlation between two consecutive acoustic-power maps, each formed by 512 frames, over the quiet region. For each filter, we have four 512-frame power maps and have three correlations between the consecutive power maps. For the raw acoustic-power maps, the correlation coefficient is less than 0.08. For the power maps with direction filter, the correlation coefficient is less than 0.14. For the power maps with direction and phase-velocity filters, the correlation coefficient is less than 0.20. The actual correlation coefficients should be less than these measured values because the large-scale nonuniformity also contributes to the measured correlations. The small correlation between consecutive power maps indicates that the spatial fluctuation patterns in the power maps change rapidly with time. The degree of randomness decreases as more filters are applied. This could be understood through the number of interference pairs in the interference term. When a filter is applied, the number of nonzero Fourier components decreases, and the number of interference pairs also decreases. This leads to a decrease in the degree of randomness for the interference term.

To test the second property, we compute the magnitude of the spatial fluctuations of the power map in the quiet region from various numbers of frames (N). The magnitude of spatial fluctuations of acoustic power in the quiet Sun is defined by the ratio of the standard deviation to the mean value. The logarithmic plot of spatial fluctuation *versus* N for three different power maps is shown in Figure 10. All three results are close to the $N^{-1/2}$ relation, which is shown by the straight line. These two tests indicate that the observed acoustic power in the quiet Sun is indeed random as predicted by Equation (3).

It should be noted that the observational noise, which is included in the power maps, may also be random with these two properties. The power spectra of observational random noise have a power law ($\propto \ell^{-\alpha}$). To check the contribution of observational noise to the spatial fluctuations of power maps in the quiet Sun, we compute the spatial power spectra of the fluctuations of power maps in the quiet Sun using different filters. The first one is the raw power map. The second power map is computed from the waves filtered with a direction filter. The third power map is computed from the waves filtered with both direction and phase-velocity filters. The spatial power spectra of the fluctuations of these three power maps of the quiet region are shown in Figure 11. These power spectra are very different from a power law. Besides the peak near $\ell = 0$, which corresponds to the large-scale nonuniformity,

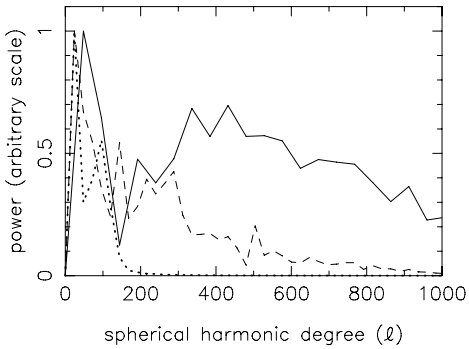

Figure 11 Spatial power spectra of the power maps of a quiet region *versus* degree ℓ. The solid line is for the raw acoustic-power map. The dashed line is for the acoustic-power map with direction filter. The dotted line is for the acoustic-power map with both direction and phase-velocity filters. The scale of power is arbitrary and is different for the different curves.

the power spectra peaks at some scale. This indicates that the contribution of observational random noise to the spatial fluctuations is relatively small.

6. Summary and Discussion

The waves filtered with the direction filter propagate in a narrow range of directions. The interaction between these waves and magnetic regions produces the extended reduced-power features behind the magnetic regions with respect to the wave direction. If the waves are further filtered with a phase-velocity filter, a reduced-power image of the sunspot, called the secondary image, appears behind the sunspot in the acoustic-power map. Since the secondary image is located outside the strong magnetic region, its Doppler measurement is not complicated by the presence of strong magnetic field. Regarding the power deficit, the secondary image contains information only in absorption and emissivity reduction in the sunspot, but not in local suppression.

The waves filtered with direction and phase-velocity filters can be used to probe the sunspot. One of examples is using the filtered waves at the location of the secondary image to measure the absorption coefficient in the leading sunspot of NOAA 9062 (Chou *et al.*, 2009). In this application, we use the property that the waves emitted along the wave path between two points have no correlation with the signal at the starting point to separate absorption from emissivity reduction in the sunspot. The wave packet travels from the starting point through the sunspot arriving at the second point after the two-skip travel distance. The second-skip cross-correlation between these two points depends on the absorption but not the emissivity reduction and local suppression in the sunspot. This allows us to determine the absorption coefficient in the sunspot.

Some other possible applications include the following: *i*) The investigation of the secondary image and the extended features with the waves propagating in different directions would help understand the interaction between the acoustic waves and magnetic fields. *ii*) The frequency dependence of the secondary image and the extended features could help understand the sunspot-induced changes in the acoustic environment around sunspots. *iii*) The phase-velocity filter dependence of the secondary image could provide depth information about the interaction between the acoustic waves and magnetic fields.

In the quiet Sun, there are spatial fluctuations in any acoustic-power map. These fluctuations are mainly caused by the interference among the modes with the same frequency. The interference pattern is determined by the filter applied to the data. The fluctuations are random with two properties: *i*) The fluctuations in two consecutive power maps have a small

correlation that indicates that they change rapidly with time. *ii*) The magnitude of the fluctuations decreases as $N^{-1/2}$. The random spatial fluctuation is one of sources of uncertainty in the measured acoustic power in both the quiet Sun and magnetic regions. It always exists even if the measured data are free of error. The only way to reduce the fluctuations from the interference is to increase the number of observed frames, N.

Acknowledgements SOHO is a project of international cooperation between ESA and NASA. We are grateful for the referee's comments and suggestions for future work. The authors were supported by the NSC of ROC under Grant No. NSC-96-2112-M-007-034-MY3.

References

Bogdan, T.J.: 1997, *Astrophys. J.* **477**, 475.
Braun, D.C.: 1995, *Astrophys. J.* **451**, 859.
Braun, D.C., Lindsey, C., Fan, Y., Jefferies, S.M.: 1992, *Astrophys. J.* **392**, 739.
Cally, P.S., Bogdan, T.J.: 1993, *Astrophys. J.* **402**, 721.
Cameron, R., Gizon, L., Duvall, T.L. Jr.: 2008, *Solar Phys.* **251**, 291.
Chou, D.-Y., Chang, H.-K., Sun, M.-T., LaBonte, B., Chen, H.-R., Yeh, S.-J., TON Team: 1999, *Astrophys. J.* **514**, 979.
Chou, D.-Y., Yang, M.-H., Liang, Z.-C., Sun, M.-T.: 2009, *Astrophys. J.* **690**, L23.
Crouch, A.D., Cally, P.S.: 2005, *Solar Phys.* **227**, 1.
Christensen-Dalagaard, J.: 2005, *Rev. Mod. Phys.* **74**(4), 1073.
Gordovskyy, M., Jain, R.: 2008, *Astrophys. J.* **681**, 664.
Hindman, B.W., Brown, T.M.: 1998, *Astrophys. J.* **504**, 1029.
Hindman, B.W., Jain, R., Zweibel, E.G.: 1997, *Astrophys. J.* **476**, 392.
Hollweg, J.V.: 1988, *Astrophys. J.* **335**, 1005.
Ladenkov, O.V., Hill, F., Egamberdiev, S.A., Chou, D.-Y.: 2002, *Astron. Lett.* **28**, 411.
Lindsey, C., Brain, D.C.: 1998, *Astrophys. J.* **499**, L99.
Lites, B.W., White, O.R., Packman, D.: 1982, *Astrophys. J.* **253**, 386.
Parchevsky, K.V., Kosovichev, A.G.: 2007, *Astrophys. J.* **666**, L53.
Rajaguru, S.P., Birch, A.C., Duvall, T.L. Jr., Thompson, M.J., Zhao, J.: 2006, *Astrophys. J.* **646**, 543.
Rajaguru, S.P., Sankarasubramanian, K., Wachter, R., Scherrer, P.H.: 2007, *Astrophys. J.* **654**, L178.
Scherrer, P.H., Bogart, R.S., Bush, R.I., Hoeksema, J.T., Kosovichev, A.G., Schou, J., Rosenberg, W., Springer, L., Tarbell, T.D., Title, A., *et al.*: 1995, *Solar Phys.* **162**, 129.
Skartlien, R.: 2002, *Astrophys. J.* **578**, 621.
Tarbell, T.D., Peri, M., Frank, Z., Shine, R., Title, A.: 1988. In: Domingo, V., Rolfe, E.J. (eds.) *Seismology of Sun and Sun-like Stars* **SP-286**, ESA, Noordwijk, 315.
Wachter, R., Schou, J., Sankarasubramanian, K.: 2006, *Astrophys. J.* **648**, 1256.
Woods, D.T., Cram, L.E.: 1981, *Solar Phys.* **69**, 233.